Energy &
Environmental Science

RSCPublishing

PAPER

View Article Online
View Journal | View Issue

Cite this: *Energy Environ. Sci.*, 2013, **6**, 2216

One-step synthesis of Ni_3S_2 nanorod@$Ni(OH)_2$ nanosheet core–shell nanostructures on a three-dimensional graphene network for high-performance supercapacitors†

Weijia Zhou,‡[abd] Xiehong Cao,‡[a] Zhiyuan Zeng,[a] Wenhui Shi,[a] Yuanyuan Zhu,[a] Qingyu Yan,[a] Hong Liu,*[bc] Jiyang Wang[b] and Hua Zhang*[a]

Received 16th January 2013
Accepted 15th May 2013

DOI: 10.1039/c3ee40155c

www.rsc.org/ees

A three-dimensional graphene network (3DGN) grown on nickel foam is an excellent template for the synthesis of graphene-based composite electrodes for use in supercapacitors. $Ni(OH)_2$ nanosheets coated onto single-crystal Ni_3S_2 nanorods grown on the surface of the 3DGN (referred to as the Ni_3S_2@$Ni(OH)_2$/3DGN) are synthesized using a one-step hydrothermal reaction. SEM, TEM, XRD and Raman spectroscopy are used to investigate the morphological and structural evolution of the Ni_3S_2@$Ni(OH)_2$/3DGN. Detailed electrochemical characterization shows that the Ni_3S_2@$Ni(OH)_2$/3DGN exhibits high specific capacitance (1277 F g^{-1} at 2 mV s^{-1} and 1037.5 F g^{-1} at 5.1 A g^{-1}) and areal capacitance (4.7 F cm^{-2} at 2 mV s^{-1} and 3.85 F cm^{-2} at 19.1 mA cm^{-2}) with good cycling performance (99.1% capacitance retention after 2000 cycles).

Introduction

The increasing demand for energy and environmental protection has stimulated intensive research into energy storage and conversion from alternative energy sources. Currently, the supercapacitor is one of the most ideal candidates for green energy storage because of its high power density, super-high cycling life and safe operation.[1–3] Based on the charge–storage mechanism, supercapacitors are generally divided into two types: electrical double-layer capacitors (EDLCs) that use carbon-active materials and pseudocapacitors that use redox-active materials. Among the numerous pseudocapacitor materials, transition metal oxides and hydroxides have been found to be excellent active materials, because of the variety of oxidation states they possess for charge transfer.[4–8] Nickel hydroxide is an especially attractive candidate for pseudocapacitors due to its layered structure, with large interlayer spacing and high theoretical specific capacitance.[9–11] However, these types of pseudocapacitors are often confronted with a compromised rate capability and reversibility, which rely on the Faradic redox reaction. Recently, metal sulfides, another kind of active material, have attracted increasing interest due to their good performance in energy storage applications[12–15] including supercapacitors.[13,15]

Two-dimensional (2D) graphene has attracted much attention due to its high surface area, high flexibility and electrical conductivity.[16–19] Graphene and graphene-based materials are widely used in electrochemical applications,[20] such as in graphene-based supercapacitors which have high specific capacitance.[21–23] Since three-dimensional (3D) nanostructures with a short path for ion diffusion and large surface area provide more efficient contact between the ions of the electrolyte and the active materials, they are seen as promising electrode materials. For example, various 3D hybrid nanostructures, such as Co_3O_4@MnO_2, CoO@NiHON and MnO_2–NiO, have been used to significantly enhance both the capacitance and durability of supercapacitors.[6,9,24]

Recently, a novel 3D graphene network (3DGN) with an enlarged void volume, large surface area and high electrical conductivity was reported.[25,26] Our previous work showed that the 3DGN grown on nickel foam is an excellent template for a

---

[a] *School of Materials Science and Engineering, Nanyang Technological University, 50 Nanyang Avenue, Singapore 639798, Singapore. E-mail: HZhang@ntu.edu.sg; Web: http://www.ntu.edu.sg/home/hzhang/*

[b] *State Key Laboratory of Crystal Materials, Center of Bio & Micro/nano Functional Materials, Shandong University, 27 Shandanan Road, Jinan 250100, China. E-mail: hongliu@sdu.edu.cn*

[c] *Beijing Institute of Nanoenergy and Nanosystems, Chinese Academy of Science, Beijing 100864, China*

[d] *New Energy Research Institute, College of Environment and Energy, South China University of Technology, Guangzhou Higher Education Mega Centre, Guangzhou 510006, China*

† Electronic supplementary information (ESI) available: Calculation methods for the specific capacitance and areal capacitance of the composite electrodes prepared, photos and SEM images of the Ni_3S_2@$Ni(OH)_2$/3DGN after the removal of Ni_3S_2@$Ni(OH)_2$ and Ni foam, TEM images of the $Ni(OH)_2$ nanosheets and Ni_3S_2@$Ni(OH)_2$ after cycling, SEM images of the untreated 3DGN and Ni_3S_2@$Ni(OH)_2$/Ni, electrochemical characterizations of Ni_3S_2/Ni, Ni_3S_2@$Ni(OH)_2$/Ni and $Ni(OH)_2$/Ni, the calculated specific capacitance and areal capacitance data for the Ni_3S_2@$Ni(OH)_2$/3DGN, and the Ragone plot of energy density (*E*) *versus* power density (*P*) of the Ni_3S_2@$Ni(OH)_2$/3DGN electrode are provided in Fig. S1–S7. See DOI: 10.1039/c3ee40155c

‡ These authors contributed equally to this work.

graphene-based composite electrode, which opened up a promising new strategy for the application of graphene-based materials in supercapacitors.[25,27] Herein, we report the growth of a novel 3D hybrid structure, *i.e.* a Ni_3S_2 nanorod@$Ni(OH)_2$ nanosheet core–shell nanostructure grown on a 3DGN on nickel foam, referred to as a Ni_3S_2@$Ni(OH)_2$/3DGN, which has robust hierarchical porosity and a high specific surface area, using a simple one-step hydrothermal reaction. The composite and nanostructure of Ni_3S_2@$Ni(OH)_2$/3DGN can be controlled by varying the reaction time and the mass ratio of Ni foam to thioacetamide (TAA). Electrochemical measurements of this novel hybrid structure exhibited a high capacitance and good cycling performance.

Experimental section

Growth of the Ni_3S_2@$Ni(OH)_2$/3DGN hybrid structure

After the three-dimensional graphene network (3DGN) was grown on a nickel foam,[25] Ni_3S_2@$Ni(OH)_2$/3DGN heterostructures were prepared using a simple one-step hydrothermal process. In a typical experiment, a piece of 3DGN on nickel foam was wrapped in Teflon tape with exposure area of ~1 cm^2, and immersed into a Teflon-lined stainless steel autoclave containing a 20 mL homogeneous solution of 25 mg thioacetamide (TAA, C_2H_5NS). The autoclave was then sealed for and the hydrothermal reaction was conducted at 180 °C for 6, 12 and 24 h in order to obtain Ni_3S_2/3DGN, Ni_3S_2@$Ni(OH)_2$/3DGN and $Ni(OH)_2$/3DGN, respectively. After the autoclave was cooled down to room temperature, the samples were rinsed with a copious amount of distilled water and then dried in an electric oven at 60 °C for 12 h. As a control experiment, the nickel foam without 3DGN was used to synthesize a Ni_3S_2 nanorod@$Ni(OH)_2$ nanosheet/nickel foam heterostructure, referred to as Ni_3S_2@$Ni(OH)_2$/Ni, at 180 °C for 12 h.

Characterization

Field emission scanning electron microscopy (FESEM, Model JSM-7600F, JEOL Ltd., Tokyo, Japan) was used to characterize the morphologies of the synthesized samples. Transmission electron microscopy (TEM) images were taken using a JOEL JEM 2100F microscope. The chemical composition was investigated by using energy dispersive X-ray spectroscopy (EDX). The X-ray powder diffraction (XRD) pattern of each sample was recorded on a Bruke D8 Advance powder X-ray diffractometer using Cu Kα radiation ($\lambda = 0.15406$ nm). Raman spectra were collected with a WITEC CRM200 Raman System (488 nm laser, 2.54 eV, WITec, Germany).

Electrochemical measurement

Cyclic voltammetry (CV) and galvanostatic charge–discharge were performed using a conventional three-electrode cell with 3 M KOH aqueous solution as the electrolyte and recorded on Solartron analytical equipment (Model 1470E, AMETEK, UK). The electrochemical impedance spectroscopy (EIS) test was performed using a conventional three-electrode system (CHI 660C, CH Instrument Inc., USA). The Ni_3S_2@$Ni(OH)_2$/3DGN on Ni foam substrate (1 cm^2), Ag/AgCl electrode (saturated KCl) and Pt wire were used as the working, reference and counter electrodes, respectively.

Results and discussion

SEM images of the obtained Ni_3S_2@$Ni(OH)_2$/3DGN (see the Experimental section for details) are shown in Fig. 1a–c. The 3DGN is covered by Ni_3S_2 nanorods with a diameter of 0.5–1 μm and a length of 5–10 μm, which grew densely and almost vertically on the surface of the 3DGN. Magnified SEM images reveal that the Ni_3S_2 nanorods are covered by $Ni(OH)_2$ nanosheets (Fig. 1c). With such a unique hierarchical structure, the space between the Ni_3S_2 nanorods in the array can be efficiently utilized, allowing the electrolyte ions easier access to the surface of the active material. The XRD spectrum of the as-grown Ni_3S_2@$Ni(OH)_2$/3DGN (Fig. 1d) shows peaks at $2\theta = 21.7$, 31.1, 37.8, 49.7 and 55.2°, which correspond to the single crystalline Ni_3S_2 (JCPDS no. 44-1418). It should be noted that two characteristic peaks for Ni at $2\theta = 44.5$ and 51.8° in the XRD pattern arise from the Ni foam substrate (JCPDS no. 65-2865). A very small amount of NiS (JCPDS no. 21-0041) is also observed in the XRD pattern. While the presence of the $Ni(OH)_2$ nanosheets was not confirmed by the XRD pattern, possibly due to there only being a tiny amount, it was confirmed from the HRTEM images and EDX (Fig. 2).

The nanostructures of the $Ni(OH)_2$ nanosheets and Ni_3S_2 nanorods were further investigated using TEM. Fig. 2a shows the typical TEM image of an individual Ni_3S_2 nanorod covered by thin $Ni(OH)_2$ nanosheets. The HRTEM image obtained from the white square area labelled (b) in Fig. 2a has a lattice spacing of 0.28 nm in the backbone area of the Ni_3S_2 nanorod (Fig. 2b), which corresponds to the (110) interplanar spacing of Ni_3S_2

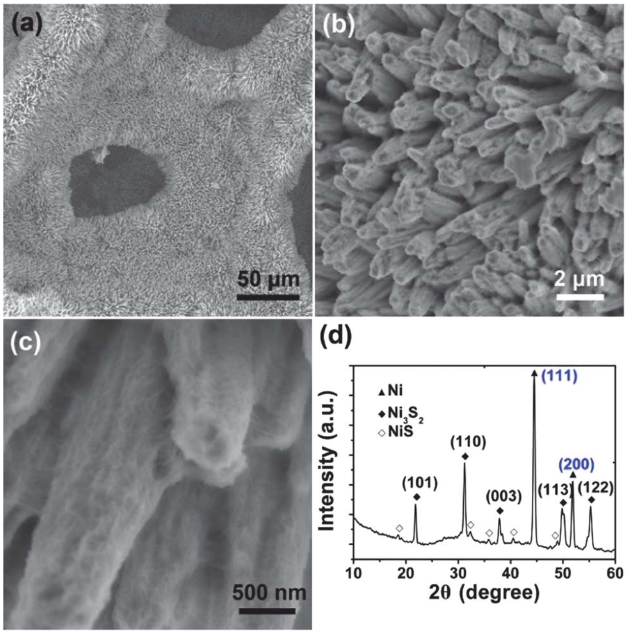

Fig. 1 (a) SEM image of Ni_3S_2@$Ni(OH)_2$/3DGN (reaction time: 12 h). (b and c) The magnified SEM images of (a). (d) XRD pattern of Ni_3S_2@$Ni(OH)_2$/3DGN.

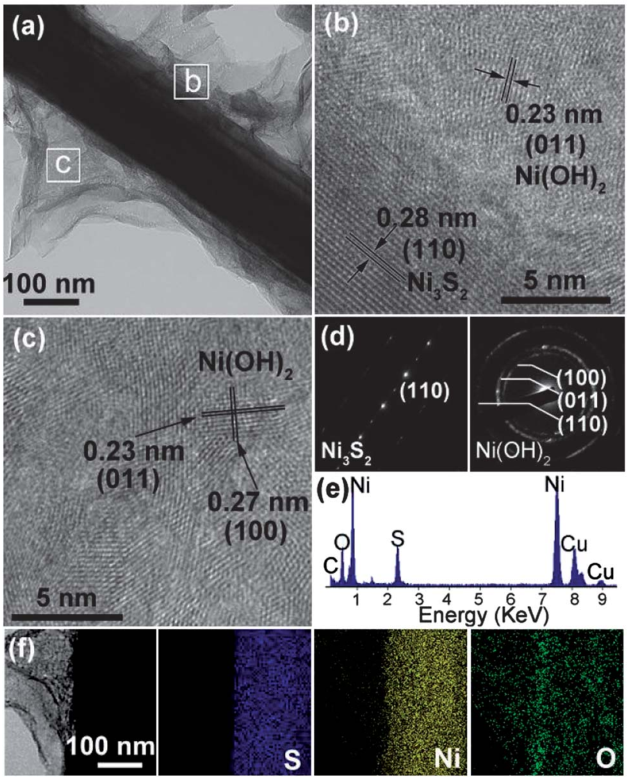

Fig. 2 (a) TEM image of Ni_3S_2@$Ni(OH)_2$. (b and c) HRTEM images of Ni_3S_2 nanorods and $Ni(OH)_2$ nanosheets from the white square areas highlighted in (a). (d) The corresponding SAED patterns of Ni_3S_2 and $Ni(OH)_2$. (e and f) EDS spectrum and mapping results from a single hybrid nanostructure, conforming to the Ni_3S_2@$Ni(OH)_2$ core–shell hierarchical structure.

(hexagonal, $a = b = 0.574$ nm, $c = 0.714$ nm). The lattice distances of 0.27 and 0.23 nm in Fig. 2c correspond to the (011) and (100) faces of $Ni(OH)_2$ (hexagonal, $a = b = 0.312$ nm, $c = 0.46$ nm). The corresponding selected-area electron diffraction (SAED) patterns (Fig. 2d) further confirmed the presence of the single crystalline Ni_3S_2 nanorods and polycrystalline $Ni(OH)_2$ nanosheets. In addition, the energy dispersive X-ray spectrometry (EDS) analysis was conducted to confirm the composition of Ni_3S_2@$Ni(OH)_2$ (Fig. 2e). The elements, Cu (from the copper TEM grid), Ni, S and O were all detected. The EDS mapping (Fig. 2f) clearly shows that the strongest signals for Ni and S were found in the backbone region, whereas only Ni and O signals were observed in the shell region, confirming the Ni_3S_2@$Ni(OH)_2$ core–shell hierarchical structure.

Raman spectroscopy was used to further characterize the synthesized Ni_3S_2@$Ni(OH)_2$/3DGN. Fig. 3 shows the typical G (~1580 cm^{-1}) and 2D (~2732 cm^{-1}) peaks that are characteristic of graphene in the 3DGN (curve a). The integrated peak area ratio of the 2D band to G band (~0.51) indicates that the 3D graphene network contains few-layer graphene.[25,26] The typical G (~1563 cm^{-1}) and 2D (~2706 cm^{-1}) peaks shown in curve b of Fig. 3 indicate that the graphene still existed after the synthesis of Ni_3S_2@$Ni(OH)_2$ on the 3DGN. In order to further confirm the presence of graphene, the Ni_2S_3@$Ni(OH)_2$ and Ni foam in Ni_3S_2@$Ni(OH)_2$/3DGN were removed by immersing Ni_3S_2@$Ni(OH)_2$/3DGN in a 1 M HCl aqueous solution at 60 °C overnight followed by rinsing with DI water several times. Fig. S1 (ESI†) indicates the 3DGN remained and 3D structure was still preserved, however some pores were observed on the surface of the graphene. In addition, two characteristic Raman peaks at ~537.6 cm^{-1} (longitudinal optical, LO) and ~1090.7 cm^{-1} (phonon modes, 2LO) were attributed to $Ni(OH)_2$ in Ni_3S_2@$Ni(OH)_2$/3DGN.[28,29]

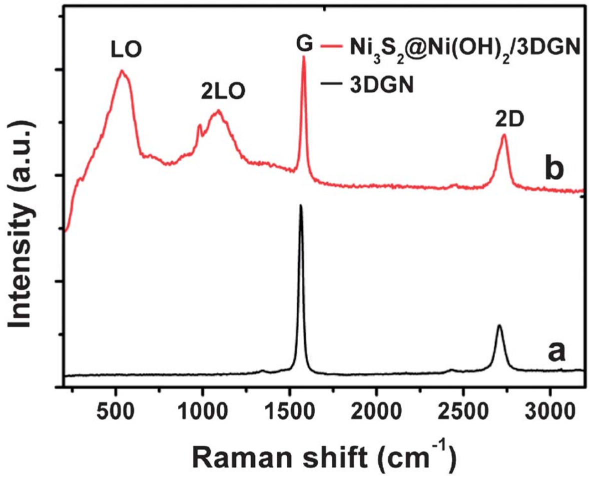

Fig. 3 Raman spectra of (a) the 3DGN and (b) the Ni_3S_2@$Ni(OH)_2$/3DGN.

To investigate the morphological and structural evolution of the Ni_3S_2@$Ni(OH)_2$/3DGN, a series of experiments with different hydrothermal reaction times were conducted (Fig. 4a–c), which indicate the evolution of the structure from Ni_3S_2 nanorods to Ni_3S_2@$Ni(OH)_2$, and then finally conversion to pure $Ni(OH)_2$ nanosheets. After a hydrothermal reaction time of 6 h, Ni_3S_2 nanorods were obtained (Fig. 4a). The XRD pattern revealed that the nanorods were of the pure spinel Ni_3S_2 phase (Fig. 4d). However, if the hydrothermal reaction was carried out for 12 h, thin nanosheets were observed on the surface of the Ni_3S_2 nanorods (Fig. 4b), which were confirmed to be $Ni(OH)_2$ using TEM, SAED patterns and the EDS spectrum as shown in Fig. 2. The $Ni(OH)_2$ nanosheets are connected to each other, forming a highly porous morphology. At a longer reaction time of 24 h, structures composed of $Ni(OH)_2$ nanosheets were observed (Fig. 4c) and the Ni_3S_2 nanorods had disappeared, which was also confirmed using TEM images (Fig. S2†). The absence of Ni_3S_2 peaks and the existence of $Ni(OH)_2$ (JCPDS no. 14-0117) peaks at $2\theta = 33$, 38.5 and 59° in the XRD spectrum (Fig. 4d) further confirmed that the Ni_3S_2 was transformed to $Ni(OH)_2$ after long reaction times (*e.g.* 24 h). Therefore, the Ni_3S_2 nanorods can be used as a sacrificial template for synthesizing the Ni_3S_2@$Ni(OH)_2$ hybrid structure using the hydrothermal reaction.

Based on the experimental results mentioned above, a possible growth mechanism for the Ni_3S_2@$Ni(OH)_2$/3DGN is proposed (Fig. 4e). It has been reported that graphene oxide can be etched by hydrothermal steaming at 200 °C, forming porous structures.[31] Therefore, we believe that the 3DGN can also be partially destroyed or etched during our hydrothermal process.

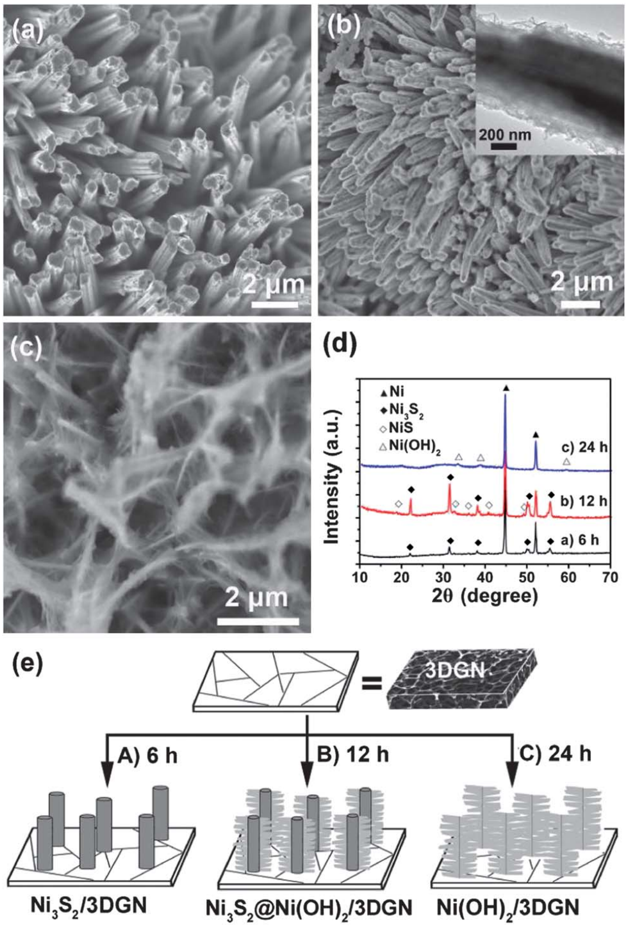

Fig. 4 SEM images of the products obtained at different hydrothermal reaction times: (a) 6 h, (b) 12 h and (c) 24 h. Inset in (b): a magnified image of the Ni_3S_2@$Ni(OH)_2$/3DGN structure. (d) The XRD patterns of the samples shown in (a–c). (e) Proposed mechanism for the growth of the Ni_3S_2@$Ni(OH)_2$/3DGN structure.

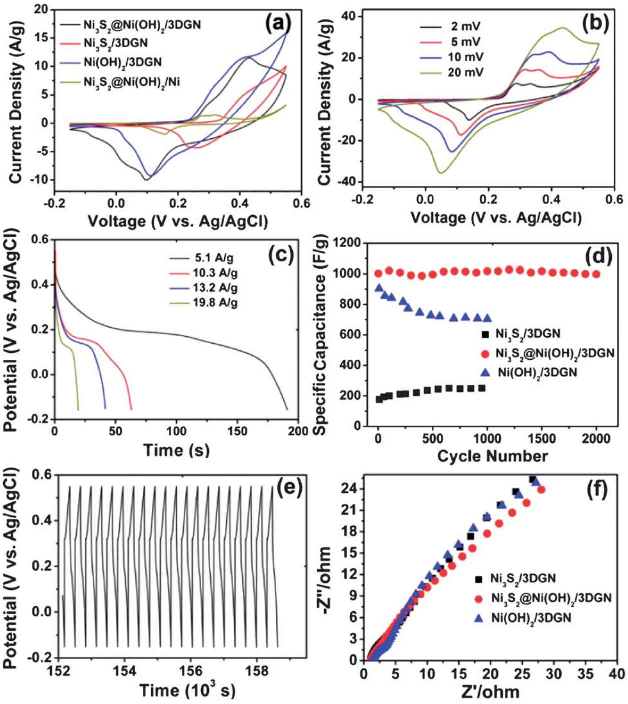

Fig. 5 (a) Cyclic voltammograms of the Ni_3S_2@$Ni(OH)_2$/3DGN, Ni_3S_2/3DGN, $Ni(OH)_2$/3DGN and Ni_3S_2@$Ni(OH)_2$/Ni foam electrodes within the potential range of −0.15 to 0.55 V at a constant scan rate of 5 mV s^{-1}. (b) Cyclic voltammograms of the Ni_3S_2@$Ni(OH)_2$/3DGN at different scan rates of 2, 5, 10 and 20 mV s^{-1}. (c) Discharge curves for the Ni_3S_2@$Ni(OH)_2$/3DGN at various current densities. (d) Cycling stability of the Ni_3S_2/3DGN, Ni_3S_2@$Ni(OH)_2$/3DGN and $Ni(OH)_2$/3DGN at a current density of 5.9 A g^{-1}. (e) The last 20 charge–discharge curves for the Ni_3S_2@$Ni(OH)_2$/3DGN. (f) Nyquist plots of the Ni_3S_2/3DGN, Ni_3S_2@$Ni(OH)_2$/3DGN and $Ni(OH)_2$/3DGN electrodes.

In this case, some of the Ni foam could be exposed. Therefore, during the hydrothermal process, the active species (S ions) released from thioacetamide (TAA) react with the exposed Ni foam to form small Ni_3S_2 particles on the surface of the 3DGN after a reaction time of 2 h (Fig. S3a and b†). The morphology obtained is different from the original 3DGN (Fig. S3c†). At longer reaction times (*e.g.* 6 h), the Ni_3S_2 nanorods grow on the surface of the 3DGN (step A in Fig. 4a and e). When the reaction time is increased to 12 h, the Ni_3S_2 nanorods are hydrolyzed under the hydrothermal conditions and the Ni_3S_2 nanorod@$Ni(OH)_2$ nanosheet core–shell heterostructure is formed (step B in Fig. 4b and e). Finally, after a reaction time of 24 h, the Ni_3S_2 nanorods are completely transformed into $Ni(OH)_2$ nanosheets (step C in Fig. 4c and e).

Fig. 5a shows the cyclic voltammogram (CV) curves of the Ni_3S_2@$Ni(OH)_2$/3DGN, Ni_3S_2/3DGN, $Ni(OH)_2$/3DGN and Ni_3S_2@$Ni(OH)_2$/nickel foam (Ni_3S_2@$Ni(OH)_2$/Ni) recorded at a scan rate of 5 mV s^{-1}. All of the CV curves exhibit a pair of redox peaks, which are distinguishable from those of electric double-layer capacitors, implying the presence of a reversible Faradic reaction and pseudocapacitive behavior. The specific capacitance of the Ni_3S_2@$Ni(OH)_2$/3DGN, $Ni(OH)_2$/3DGN and Ni_3S_2/3DGN calculated from CV curves at 5 mV s^{-1} were 1125, 981 and 340 F g^{-1}, respectively (for detailed calculations see the ESI†), which are higher than those of the composites directly grown on Ni foam without the 3DGN (*i.e.* Ni_3S_2@$Ni(OH)_2$/Ni, Ni_3S_2/Ni and $Ni(OH)_2$/Ni, Fig. S4†). This indicates that the 3DGN on the surface of the nickel foam plays an essential role in enhancing the supercapacitor performance. Importantly, the greatly enhanced electrochemical behavior of the Ni_3S_2@$Ni(OH)_2$/3DGN, compared with the $Ni(OH)_2$/3DGN and Ni_3S_2/3DGN, can be attributed to the synergistic effect resulting from the more active sites offered by the $Ni(OH)_2$ nanosheets and the quick electron transport of the highly crystalline Ni_3S_2 nanorods.[6,32]

Fig. 5b shows the CV curves of the Ni_3S_2@$Ni(OH)_2$/3DGN at different scan rates. With the increase of scan rate, the current response increases accordingly and the shapes of CV curves are retained, indicating a good rate capability. The specific capacitance of the Ni_3S_2@$Ni(OH)_2$/3DGN calculated from the CV curve is 1277 F g^{-1} at a scan rate of 2 mV s^{-1} and 716 F g^{-1} at a high scan rate of 20 mV s^{-1} (Fig. S5a†). Fig. 5c shows the galvanostatic discharge curves of the Ni_3S_2@$Ni(OH)_2$/3DGN at different current densities. A high specific capacitance (1037.5 F g^{-1}) was obtained at a discharge current density of 5.1 A g^{-1}. Even at a relatively high current density of 19.8 A g^{-1}, a specific capacitance of 398 F g^{-1} was obtained (Fig. S5b†). It should be noted that the aforementioned capacitance values of the composite electrodes (*e.g.* the Ni_3S_2@$Ni(OH)_2$/3DGN and Ni_3S_2@$Ni(OH)_2$/Ni) were calculated based on Ni_3S_2 (for detailed calculations, see the ESI†), since the exact mass ratio of Ni_3S_2 and $Ni(OH)_2$ is difficult to determine. Therefore, the actual capacitance value of the Ni_3S_2@$Ni(OH)_2$/3DGN structure should be higher than the aforementioned value, *e.g.* 1724 F g^{-1} at 2 mV s^{-1} and 1402 F g^{-1} at 5.1 A g^{-1} are the calculated values based on $Ni(OH)_2$ (Fig. S5†).

The cycling performances of the Ni_3S_2@$Ni(OH)_2$/3DGN, $Ni(OH)_2$/3DGN and Ni_3S_2/3DGN at a current density of 5.9 A g^{-1} are shown in Fig. 5d. At this current density, the specific capacitance of 981 F g^{-1} (99.1% of the initial value of 1003 F g^{-1}), calculated based on the pure Ni_3S_2, can be maintained after 2000 cycles. The shape of the last 20 charge–discharge curves (Fig. 5e) and the morphology of Ni_3S_2@$Ni(OH)_2$ after 2000 cycles (Fig. S6†) are nearly unchanged, indicating the excellent cyclability of the Ni_3S_2@$Ni(OH)_2$/3DGN electrode. However, the Ni_3S_2/3DGN shows a relatively low specific capacitance of 177 F g^{-1} for the first cycle. The specific capacitance increased slightly in subsequent cycles, possibly due to the formation of $Ni(OH)_2$ on the surface of the Ni_3S_2 nanorods while in the alkaline solution.[33,34] While the $Ni(OH)_2$/3DGN possesses a specific capacitance of 903 F g^{-1} for the first charge–discharge cycle, its specific capacitance decreases to 704 F g^{-1} (78% of the initial value) after 1000 cycles. The relatively worse cycling performance of $Ni(OH)_2$ is similar to that seen in previous reports.[29,30] Importantly, our Ni_3S_2@$Ni(OH)_2$/3DGN electrode shows higher specific capacitance than many of the previously reported composite electrodes including CoO@NiHON (798.3 F g^{-1} at 1.67 A g^{-1}, 95% maintained after 2000 cycles),[9] NiS hollow sphere (927 F g^{-1} at 4.08 A g^{-1}, 70% maintained after 3000 cycles)[15] and NiO/3D graphene (745 F g^{-1} at 1.4 A g^{-1}, 100% maintained after 2000 cycles)[25] electrodes. In addition, electrochemical impedance spectroscopy (EIS) was also employed to characterize the composite electrodes (Fig. 5f). The equivalent series resistance (ESR) values of the Ni_3S_2/3DGN, Ni_3S_2@$Ni(OH)_2$/3DGN and $Ni(OH)_2$/3DGN are 1.07, 1.13 and 1.33 Ω, respectively, which are smaller than that reported for $Ni(OH)_2$-coated nickel foam electrodes with high capacitive performance.[35] Compared to the aforementioned 3DGN-based composites, Ni_3S_2@$Ni(OH)_2$/Ni has a higher ESR value (4.57 Ω), indicating that the 3DGN improved the charge transport properties of the composite electrodes (Fig. S4d†).

Fabrication of electrodes with high mass loading of active materials has practical significance in supercapacitor devices.[36,37] However, the increase in loading density often results in a decrease of the performance of these electrochemical devices.[38] Fortunately, our Ni_3S_2@$Ni(OH)_2$/3DGN electrode with a high loading density (~3.7 mg cm^{-2}) still exhibits excellent supercapacitor performance as mentioned above. Moreover, the high areal capacitance of the Ni_3S_2@$Ni(OH)_2$/3DGN is 4.7 F cm^{-2} at 2 mV s^{-1} and 3.85 F cm^{-2} at 19.1 mA cm^{-2} (Fig. S5†), which is much better than the reported values for materials based on Co_3O_4@MnO_2 (0.56 F cm^{-2} at 11.25 mA cm^{-2}),[6] MnO_2/carbon nanotubes (2.8 F cm^{-2} at 0.05 mV s^{-1})[38] and Co_3O_4/NiO (2.56 F cm^{-2} at 2 A g^{-1}).[39] To further evaluate the performance of the Ni_3S_2@$Ni(OH)_2$/3DGN electrode, the energy density (*E*) and power density (*P*) were calculated from the charge–discharge curves (see the ESI† for the details). The Ni_3S_2@$Ni(OH)_2$/3DGN gave a high energy density of 70.6 Wh kg^{-1} at a power density of 1.3 kW kg^{-1}, and still retains a value of 27.1 Wh kg^{-1} at a power density of 5 kW kg^{-1} (Fig. S7†).

The aforementioned results reveal the high specific capacitance, remarkable rate capability as well as excellent cycling performance of the Ni_3S_2@$Ni(OH)_2$/3DGN when used as high-performance electrochemical pseudocapacitors. Such superior performance of the Ni_3S_2@$Ni(OH)_2$/3DGN can be attributed to the following factors. First, the CVD grown 3DGN on nickel foam with a high surface area and high electrical conductivity can effectively collect and transfer charges.[25,27] Second, the $Ni(OH)_2$ nanosheets possess a high contact area with the electrolyte, thus enabling fast and reversible redox reactions, which improve the specific capacitance.[9,35] Third, the single-crystal Ni_3S_2 nanorod array grown on the surface of the 3DGN provides large open spaces and a shorter ion diffusion path, which avoid the use of a polymer binder or conductive additive in the electrode materials.[6,40] Importantly, Ni_3S_2 has a heazlewoodite structure with short metal–metal distances in an approximately body-centred cubic sulphur lattice, which results in it having good electrical properties[33] and enables the quick transport of electrons along the Ni_3S_2 nanorods. In addition, the one-step synthesized Ni_3S_2@$Ni(OH)_2$ core–shell nanostructures on the 3DGN aids the electron transfer between the $Ni(OH)_2$, Ni_3S_2 and 3DGN components due to the perfect interface connection between them.

Conclusions

In summary, the large-amount Ni_3S_2@$Ni(OH)_2$/3DGN, *i.e.* $Ni(OH)_2$ nanosheets coated on the single-crystal Ni_3S_2 nanorods grown on the surface of 3D graphene network, is synthesized by a simple one-step hydrothermal reaction. By controlling the reaction time, different composites and nanostructures, *i.e.*, Ni_3S_2/3DGN, Ni_3S_2@$Ni(OH)_2$/3DGN and $Ni(OH)_2$/3DGN, are obtained. Detailed electrochemical characterization shows that the Ni_3S_2@$Ni(OH)_2$/3DGN exhibits high specific capacitance (1277 F g^{-1} at 2 mV s^{-1} and 1037.5 F g^{-1} at 5.1 A g^{-1}) and areal capacitance (4.7 F cm^{-2} at 2 mV s^{-1} and 3.85 F cm^{-2} at 19.1 mA cm^{-2}) with good cycling performance (99.1% capacitance retention after 2000 cycles). The enhanced supercapacitor performance might arise from the synergistic effect between the $Ni(OH)_2$ nanosheets, Ni_3S_2 nanorods and 3D graphene network.

Acknowledgements

This work was supported by MOE under AcRF Tier 2 (ARC 10/10, no. MOE2010-T2-1-060) and AcRF Tier 1 (2012-T1-001-161), Start-Up Grant (M4080865.070.706022) in NTU. This research is also funded by the Singapore National Research Foundation and the publication is supported under the Campus for

Research Excellence And Technological Enterprise (CREATE) programme. H. L. thanks the support from the NSFDYS: 50925205 in Shandong University in China, the National Natural Science Foundation of China (NSFDYS: 50925205), and the "100 Talents Program" of Chinese Academy of Sciences.

Notes and references

1 J. R. Miller and P. Simon, *Science*, 2008, **321**, 651.
2 P. Simon and Y. Gogotsi, *Nat. Mater.*, 2008, **7**, 845.
3 J. Jiang, J. P. Liu, W. W. Zhou, J. H. Zhu, X. T. Huang, X. Y. Qi, H. Zhang and T. Yu, *Energy Environ. Sci.*, 2011, **4**, 5000.
4 S. Chen, J. W. Zhu, X. D. Wu, Q. F. Han and X. Wang, *ACS Nano*, 2010, **4**, 2822.
5 K. Xie, J. Li, Y. Q. Lai, W. Lu, Z. Zhang, Y. X. Liu, L. Zhou and H. T. Huang, *Electrochem. Commun.*, 2011, **13**, 657.
6 J. P. Liu, J. Jiang, C. W. Cheng, H. X. Li, J. X. Zhang, H. Gong and H. J. Fan, *Adv. Mater.*, 2011, **23**, 2076.
7 H. L. Wang, H. S. Casalongue, Y. Y. Liang and H. J. Dai, *J. Am. Chem. Soc.*, 2010, **132**, 7472.
8 C. C. Hu, K. H. Chang, M. C. Lin and Y. T. Wu, *Nano Lett.*, 2006, **6**, 2690.
9 C. Guan, J. P. Liu, C. W. Cheng, H. X. Li, X. L. Li, W. W. Zhou, H. Zhang and H. J. Fan, *Energy Environ. Sci.*, 2011, **4**, 4496.
10 F. S. Cai, G. Y. Zhang, J. Chen, X. L. Gou, H. K. Liu and S. X. Dou, *Angew. Chem., Int. Ed.*, 2004, **43**, 4212.
11 S. B. Yang, X. L. Wu, C. L. Chen, H. L. Dong, W. P. Hu and X. K. Wang, *Chem. Commun.*, 2012, **48**, 2773.
12 Y. P. Du, Z. Y. Yin, J. X. Zhu, X. Huang, X. J. Wu, Z. Y. Zeng, Q. Y. Yan and H. Zhang, *Nat. Commun.*, 2012, **3**, 1177.
13 F. Tao, Y. Q. Zhao, G. Q. Zhang and H. L. Li, *Electrochem. Commun.*, 2007, **9**, 1282.
14 S. J. Bao, C. M. Li, C. X. Guo and Y. Qiao, *J. Power Sources*, 2006, **159**, 287.
15 T. Zhu, Z. Y. Wang, S. J. Ding, J. S. Chen and X. W. Lou, *RSC Adv.*, 2011, **1**, 397.
16 W. S. Hummers and R. E. Offeman, *J. Am. Chem. Soc.*, 1958, **80**, 1339.
17 S. Stankovich, D. A. Dikin, G. H. B. Dommett, K. M. Kohlhaas, E. J. Zimney, E. A. Stach, R. D. Piner, S. T. Nguyen and R. S. Ruoff, *Nature*, 2006, **442**, 282.
18 X. Huang, X. Y. Qi, F. Boey and H. Zhang, *Chem. Soc. Rev.*, 2012, **41**, 666.
19 X. Huang, Z. Y. Yin, S. X. Wu, X. Y. Qi, Q. Y. He, Q. C. Zhang, Q. Y. Yan, F. Boey and H. Zhang, *Small*, 2011, **7**, 1876.
20 (*a*) S. X. Wu, Q. Y. He, C. L. Tan, Y. D. Wang and H. Zhang, *Small*, 2013, **9**, 1160; (*b*) K. Chang and W. X. Chen, *ACS Nano*, 2011, **5**, 4720.
21 Y. W. Zhu, S. Murali, M. D. Stoller, K. J. Ganesh, W. W. Cai, P. J. Ferreira, A. Pirkle, R. M. Wallace, K. A. Cychosz, M. Thommes, D. Su, E. A. Stach and R. S. Ruoff, *Science*, 2011, **332**, 1537.
22 M. D. Stoller, S. Park, Y. W. Zhu, J. An and R. S. Ruoff, *Nano Lett.*, 2008, **8**, 3498.
23 G. H. Yu, L. B. Hu, N. Liu, H. L. Wang, M. Vosgueritchian, Y. Yang, Y. Cui and Z. N. Bao, *Nano Lett.*, 2011, **11**, 4438.
24 J. P. Liu, J. Jiang, M. Bosmanc and H. J. Fan, *J. Mater. Chem.*, 2012, **22**, 2419.
25 X. H. Cao, Y. M. Shi, W. H. Shi, G. Lu, X. Huang, Q. Y. Yan, Q. C. Zhang and H. Zhang, *Small*, 2011, **7**, 3163.
26 Z. P. Chen, W. C. Ren, L. B. Gao, B. L. Liu, S. F. Pei and H. M. Cheng, *Nat. Mater.*, 2011, **10**, 424.
27 X. C. Dong, H. Xu, X. W. Wang, Y. X. Huang, M. B. C. Park, H. Zhang, L. H. Wang, W. Huang and P. Chen, *ACS Nano*, 2012, **6**, 3206.
28 G. D. Zhou, D. W. Wang, L. C. Yin, N. Li, F. Li and H. M. Cheng, *ACS Nano*, 2012, **6**, 3214.
29 J. Yan, W. Sun, T. Wei, Q. Zhang, Z. J. Fan and F. Wei, *J. Mater. Chem.*, 2012, **22**, 11494.
30 B. Zhao, J. S. Song, P. Liu, W. W. Xu, T. Fang, Z. Jiao, H. J. Zhang and Y. Jiang, *J. Mater. Chem.*, 2011, **21**, 18792.
31 T. H. Han, Y. K. Huang, A. T. L. Tan, V. P. Dravid and J. X. Huang, *J. Am. Chem. Soc.*, 2011, **133**, 15264.
32 C. H. Lai, K. W. Huang, J. H. Cheng, C. Y. Lee, W. F. Lee, C. T. Huang, B. J. Hwang and L. J. Chen, *J. Mater. Chem.*, 2009, **19**, 7277.
33 A. N. Buckley and R. Woods, *J. Appl. Electrochem.*, 1991, **21**, 575.
34 B. Zhang, X. C. Ye, W. Dai, W. Y. Hou and Y. Xie, *Chem.–Eur. J.*, 2006, **12**, 2337.
35 G. W. Yang, C. L. Xu and H. L. Li, *Chem. Commun.*, 2008, 6537.
36 M. D. Stoller and R. S. Ruoff, *Energy Environ. Sci.*, 2010, **3**, 1294.
37 G. H. Yu, L. B. Hu, M. Vosgueritchian, H. L. Wang, X. Xie, J. R. McDonough, X. Cui, Y. Cui and Z. N. Bao, *Nano Lett.*, 2011, **11**, 2905.
38 L. B. Hu, W. Chen, X. Xie, N. Liu, Y. Yang, H. Wu, Y. Yao, M. Pasta, H. N. Alshareef and Y. Cui, *ACS Nano*, 2011, **5**, 8904.
39 X. H. Xia, J. P. Tu, Y. Q. Zhang, X. L. Wang, C. D. Gu, X. B. Zhao and H. J. Fan, *ACS Nano*, 2012, **6**, 5531.
40 Y. G. Li, B. Tan and Y. Y. Wu, *Nano Lett.*, 2008, **8**, 265–270.